

Graphene doping to enhance flux pinning and supercurrent carrying ability in magnesium diboride superconductor

X. Xu, S. X. Dou,^{a)} X. L. Wang, J. H. Kim

Institute for Superconducting & Electronic Materials, University of Wollongong, Wollongong, NSW, 2522, Australia

J. A. Stride, M. Choucair

*School of Chemistry, University of New South Wales, Sydney, NSW 2052, Australia
Australian Nuclear Science and Technology Organisation, PMB 1, Menai, NSW 2234, Australia*

W. K. Yeoh, R. K. Zheng, S. P. Ringer

Electron Microscope Unit, University of Sydney, NSW 2052, Australia

It has been shown that graphene doping is sufficient to lead to an improvement in the critical current density - field performance ($J_c(B)$), with little change in the transition temperature in MgB₂. At 3.7 at% graphene doping of MgB₂ an optimal enhancement in $J_c(B)$ was reached by a factor of 30 at 5 K and 10 T, compared to the un-doped sample. The results suggested that effective carbon substitutions by grapheme, 2D nature of grapheme and the strain effect induced by difference thermal coefficient between single grapheme sheet and MgB₂ superconductor may play an important role in flux pinning enhancement.

Correspondence and requests for materials should be addressed to S. X. Dou (shi_dou@uow.edu.au)

Substitutional chemistry can modify, in a controlled way, the electronic structures of superconductors and their superconducting properties, such as the transition temperature (T_c), critical current density (J_c), upper critical field (H_{c2}), and irreversibility field (H_{irr}). In particular, carbon containing dopants, including nano-meter sized carbon (nano-C), silicon carbide (SiC), carbon nanotubes (CNTs), hydrocarbons/carbohydrates, and graphite are effective means to enhance the J_c - field dependence and H_{c2} ¹⁻¹¹. In this work, it will be seen the graphene as one kind of carbon source dopant, how it is useful to incorporation into MgB₂ and it is expected that H_{c2} and the flux pinning properties should be improved. However, until now there has been no report on the effects of graphene doping on the superconductivity of MgB₂, partly due to the unavailability of graphene on a suitable scale. Recently, high-throughput solution processing of large-scale graphene has been reported by a number of groups¹²⁻¹⁷.

Based on the works of Choucair *et al.*¹⁸, sufficient quantities of graphene were obtained for doping the bulk MgB₂ samples via a diffusion process. The crystalline Boron powder (0.2 to 2.4 μm) 99.999% without and with graphene¹⁸ was prepared by ball milling with toluene medium. Then the powders were dried in a vacuum oven to evaporate the medium. These powders were mixed and pressed into pellets. The pellets were then put into an iron tube filled with Mg powder (-325mesh 99%). The samples were sintered at 850°C for 10 hrs in a quartz tube; the heating rate was 5°Cmin⁻¹ under high purity argon (Ar 99.9%) gas. The phase and crystal structure of all the samples were investigated by X-ray diffraction (XRD). T_c was defined as the onset temperature at which diamagnetic properties were observed. The magnetic J_c was derived from the width of the magnetization loop using Bean's model by a Physical Properties Measurement System (PPMS). Transport measurements for resistivity (ρ) were done using a standard AC four probe method. In addition, $H_{c2}(T)$ and $H_{irr}(T)$ were defined as the fields where the temperature dependent resistance at constant magnetic field $R(H_{c2}, T) = 0.9R_{ns}$ and $R(H_{irr}, T) = 0.1R_{ns}$ with R_{ns} being the normal state resistance near 40 K.

The common format Mg(B_{1-x}C_x), x=0, 0.037, and 0.087 was used. The composition of graphene doped MgB₂ were 0, 3.7, and 8.7 at%, and as such, the sample names are designated as G000, G037, and G087, respectively. We demonstrate that the graphene doping can result a greater enhancement of the critical

current density (J_c) by over one order of magnitude in high magnetic fields. The J_c achieved is as high as $2.0 \times 10^4 \text{ Acm}^{-2}$ at 5 K and 8 T magnetic field for a graphene dopant level of only 3.7 at%, with only a slight corresponding drop in T_c . This improvement is likely caused by the following factors: the single carbon sheet with two dimensional (2-D) geometry, the negative thermal expansion coefficient, and high thermal conductivity. However, further studies are needed to clarify the dominating mechanisms responsible for the enhancement.

The lattice parameters, a , c , the ratio of a/c , grain size, strain, and full width at half maximum of the representative peak (110) calculated from the XRD patterns are shown in Table 1. Both the a -axis and c -axis parameters vary little with increasing graphene doping level of 3.7%, apart from G087 sample, which shows a notable decrease in the a -axis parameter, suggesting that carbon (C) is likely to be partially substituted into the boron (B) sites, leading to a slight drop in T_c (36.7 K) for the G087 sample. We also observed that the full width at half maximum (FWHM) of the (110) peak increases gradually with increasing graphene dopant level. Such a peak broadening is caused by both grain size reduction and an increase in lattice strain. The calculated results on grain size and lattice strain from a Williamson-Hall plot¹⁸ are given in Table 1. Also, the T_c onset determined from the AC susceptibility measurement is 38.9 K for the un-doped sample, dropping only slightly to 37.7 and 36.7 K for the G037 and G087 samples, respectively.

The temperature dependence of the resistivity (ρ) measured in different fields is shown in Fig. 1. The graphene doped samples have higher resistivity than the un-doped MgB_2 sample, indicating that electron scattering occurs at higher doping levels to some extent. However, it should be pointed out that the increase in resistivity is much smaller than for any other forms of carbon doped MgB_2 ¹⁻⁹. The J_c is actually greatly enhanced in high magnetic fields for the graphene doped samples due to enhanced flux pinning.

Fig. 2 shows the $J_c(B)$ curves at 5 K and 20K for all the samples, which were sintered at 850°C for 10 hours. The $J_c(B)$ values for all the doped samples are higher than the un-doped sample at high fields. The sample G037 gives the highest J_c at high fields: J_c increases by a factor of 30 at 5 K for the field of 10 T, as compared to the un-doped sample, G000. Even though the J_c in the low field regime is depressed, a higher doping level (G087), still results in the rate of J_c dropping much slower than the un-doped sample,

clearly indicating strong flux pinning induced by the graphene doping. The most significant effect of graphene doping is the high effectiveness of graphene to improve flux pinning at lower doping levels, which distinguishes graphene from any other C containing dopants, for example, the J_c for G037 reached 20,000 A/cm² at 5 K and 8 T, exceeding or matching the best J_c resulting from dopants such as SiC, CNT, and carbohydrates at their optimal doping level of 10 at%^{1,2,5-8}, as well as nano-C at its optimal doping level of 5-6.4 at%^{3,4,9,10}. In the latter case, T_c is noticeably reduced to temperatures as low as 30 K. Compared to the graphite doped MgB₂ pellets prepared through the ball-milling and HIP the J_c of graphite doping is better than graphene doping at 5 K¹¹, but at 20K, the graphene doping is much better than graphite, for example, the J_c is more than 500 A/cm² at 6T for graphene doped while only 10 A/cm² for graphite doped MgB₂¹¹. In comparison, low levels of graphene doping have little effect on T_c and cause only a very small increase in impurities, not compromising the significant enhancement in J_c in high fields by the degradation in low-field J_c , which is a common issue for all other C based dopants. In order to see the difference with other C based dopant, the same preparation route was applied to 5 at% nano-C doped sample and the resultant decrease in J_c at 20K can be seen in the Fig. 2, This is because the T_c is only 34K for this sample.

Fig. 3 shows the upper critical field, H_{c2} , and the irreversibility field, H_{irr} , versus the normalised T_c for all the samples. It should be noted that both H_{c2} and H_{irr} are increased by graphene doping. This indicates that graphene doping gives a much stronger improvement in flux pinning than in the upper critical field. The latter is closely related to the carbon substituting for B.

The mechanism for enhancement of J_c , H_{irr} , and H_{c2} by carbon containing dopants has been well studied. The C can enter the MgB₂ structure by substituting into B sites, and thus J_c and H_{c2} are significantly enhanced due to the increased impurity scattering in the two-band MgB₂²⁰. Above all, C substitution induces highly localised fluctuations in the structure and T_c , which have also been seen to be responsible for the enhancements in J_c , H_{irr} , and H_{c2} by SiC doping¹. Furthermore, residual thermal strain in the MgB₂-dopant composites can also contribute to the improvement in flux pinning²¹. In the present work, the C substitution for B (up to 3.7 at.%) graphene doping is lower, from the table 1, the change of the a-parameter is too smaller, according to Avdeev *et al* result²², the level of C substitution, x in the

formula $\text{Mg}(\text{B}_{1-x}\text{C}_x)$, can be estimated as $x=7.5 \times \Delta(c/a)$, where $\Delta(c/a)$ is the change in c/a compared to a pure sample. If there is any at all - as both the a -axis and the c -axis lattice parameters determined from the XRD data showed little change within this doping range. This is in good agreement with the small reduction in T_c over this doping regime. At 8.7 at% doping, there is a noticeable drop in the a -axis parameter, suggesting C substitution for B, which is also consistent with the reduction in T_c . The source of C could be the edges of the graphene sheets, although the graphene is very stable at the sintering temperature (850°C), as there have been reports of graphene formation on substrates at temperatures ranging from 870-1320°C²³.

The significant enhancement in J_c and H_{irr} for G037 can not be explained by C substitution only. The strict 2-D nature of graphene in irregular shapes may make the sheets strong pinning centres. It is also important to note that the coefficient of thermal expansion for graphene is negative^{24,25} up to 2300 K, while for MgB_2 , this is not only very large, but highly anisotropic, with a larger coefficient of thermal expansion in the c -axis direction from room temperature to 900°C²⁶. Upon cooling, MgB_2 is subjected to high tensile strain, a consequence of the graphene expanding in accordance with the negative coefficient of thermal expansion. As a result, the large strain along the graphene sheet will induce defects in MgB_2 , contributing to the enhancement in flux pinning and H_{irr} . The strain induced enhancement of flux pinning was also observed in coated superconductors²⁷ due to lattice mismatch and in SiC- MgB_2 composites as a result of residual thermal strain²¹. In the case of SiC- MgB_2 composite, the coefficient of thermal expansion for SiC is not negative, but is smaller than that of MgB_2 . Whilst graphene has a negative coefficient of thermal expansion and hence a larger effect on strain, a larger extent of defects is expected in graphene doped MgB_2 .

The microstructure revealed by high resolution transmission electron microscope (TEM) observations show that G037 sample has grain size of 100-200 nm which is consistent with value of the calculated grain size in table 1. The graphene doped samples have relatively higher density of defects compared with the undoped sample under TEM images as shown in figure 4(a) and (c). The density of such defects is estimated to be 1/3 areas of TEM images, indicating high density in the doped samples. In Figures 4(b) it should be noted that the order of fringes varies from grain to grain, indicates that the defect is due to highly

anisotropic of the interface. Similar fringes have been reported in the MgB_2 ²¹ where these fringes were induced by tensile stress with dislocations and distortions which were commonly observed in the areas. As the graphene doped samples were sintered at 850°C for 10 hrs, the samples are expected to be relatively crystalline and contain few defects. The large amount of defects and amorphous phases on the nanoscale can also be attributed to the residual thermal strain between the graphene and the MgB_2 after cooling. Defects on the order of the coherence length of the beam, ξ , can also play a role as effective pinning centres that are responsible for the enhanced flux pinning and J_c in the graphene doped MgB_2 .

In summary, the effects of graphene doping on the lattice parameters, T_c , J_c , and flux pinning in MgB_2 were investigated over a range of low doping levels. It was found that substitution of C for B enhances the flux pinning slightly depressing T_c . By controlling the processing parameters, an optimised $J_c(B)$ performance is achieved at a doping level of 3.7 at.%. Under these conditions, J_c was enhanced by an order of magnitude at 8 T and 5 K. The combination of the 2-D geometry of graphene, low C substitution for B, and in particular, residual thermal strain effects between graphene and MgB_2 are proposed to be responsible for the enhancement of flux pinning in high fields. The strong enhancement of J_c , H_{c2} , and H_{irr} with low levels of graphene doping is promising for large-scale MgB_2 wire applications.

References:

1. S. X. Dou, S. Soltanian, J. Horvat, X. L. Wang, S. H. Zhou, M. Ionescu, H. K. Liu, P. Munroe, and M. Tomsic, *Appl. Phys. Lett.* **81**, 3419 (2002).
2. S. X. Dou, O. Shcherbakova, W. K. Yeoh, J. H. Kim, S. Soltanian, X. L. Wang, C. Senatore, R. Flukiger, M. Dhalle, O. Husnjak, and E. Babic, *Phys. Rev. Lett.* **98**, 097002-1 (2007).
3. Y. Ma, X. Zhang, G. Nishijima, K. Watanabe, S. Awaji, and X. Bai, *Appl. Phys. Lett.* **88**, 072502 (2006).
4. B. J. Senkowicz, J. E. Giencke, S. Patnaik, C. B. Eom, E. E. Hellstrom, and D. C. Larbalestier, *Appl. Phys. Lett.* **86**, 202502 (2005).
5. H. Kumakura, H. Kitaguchi, A. Matsumoto, and H. Hatakeyama, *Appl. Phys. Lett.* **84**, 3669-3671 (2004).
6. M. D. Sumption, M. Bhatia, M. Rindfleisch, M. Tomsic, S. Soltanian, S. X. Dou, and E. W. Collings, *Appl. Phys. Lett.* **86**, 092507 (2005).
7. S. X. Dou, W. K. Yeoh, J. Horvat, and M. Ionescu, *Appl. Phys. Lett.* **83**, 4996 (2003).
8. J. H. Kim, S. Zhou, M. S. A. Hossain, A. V. Pan, and S. X. Dou, *Appl. Phys. Lett.* **89**, 142505 (2006).
9. R. H. T. Wilke, S. L. Bud'ko, P. C. Canfield, D. K. Finnemore, R. J. Suplinskas, and S. T. Hannahs, *Phys. Rev. Lett.* **92**, 217003 (2004).
10. W. Häßler, M. Herrmann, C. Rodig, M. Schubert, K. Nenkov, and B. Holzapfel, *Supercond. Sci. Technol.* **21**, R17 (2003).
11. B. J. Senkowicz, J. E. Giencke, S. Patnaik, C. B. Eom, E. E. Hellstrom, and D. C. Larbalestier, *Appl. Phys. Lett.* **86**, 202502 (2005).
12. V. C. Tung, M. J. Allen, Y. Yang, and R. B. Kaner, *Nature Nanotech.* **4**, 25-29 (2009).
13. K. S. Kim, Y. Zhao, H. Jang, S. Y. Lee, J. M. Kim, K. S. Kim, J. H. Ahn, P. Kim, J. Y. Choi, and B. H. Hong, *Nature* **457**, 706-710 (2009).

14. Y. Hernandez, V. Nicolosi, M. Lotya, F. M. Blighe, Z. Sun, S. De, I. T. McGovern, B. Holland, M. Byrne, Y. K. Gun'Ko, J. J. Boland, P. Niraj, G. Duesberg, S. Krishnamurthy, R. Goodhue, J. Hutchison, V. Scardaci, A. C. Ferrari, and J. N. Coleman, *Nature Nanotech.* **3**, 563–568 (2008).
15. D. Li, M. B. Müller, S. Gilje, R. B. Kaner, and G. G. Wallace, *Nature Nanotech.* **3**, 101–105 (2008).
16. X. Li, X. Wang, L. Zhang, S. Lee, and H. Dai, *Science* **319**, 1229–1232 (2008).
17. S. Stankovich, D. A. Dikin, R. D. Piner, K. A. Kohlhaas, A. Kleinhammes, Y. Jia, Y. Wu, S. T. Nguyen, and R. S. Ruoff, *Carbon* **45**, 1558–1565 (2007).
18. M. Choucair, P. Thordarson, and J. A. Stride, *Nature Nanotech.* **4**, 30-33 (2009).
19. G. K. Williamson, and W. H. Hall, *Acta Metall.* **1**, 22-31 (1953).
20. A. Gurevich, *Phys. Rev. B* **67**, 184515 (2003).
21. R. Zeng, S. X. Dou, L. Lu, W. X. Li, J. H. Kim, P. Munroe, R. K. Zheng, and S. P. Ringer, *Appl. Phys. Lett.* **94**, 042510 (2009).
22. M. Avdeev, J. D. Jorgensen, R. A. Ribeiro, S. L. Bud'ko, and P. C. Canfield, *Physica C* **387** 301-306, (2003).
23. J. Coraux, A. T. N'Diaye, M. Engler, C. Busse, D. Wall, N. Buckanie, F. M. Heringdorf, R. Gastel, B. Poelsema, and T. Michely, *New J. Phys.* **11**, 023006 (2009).
24. N. Mounet, and N. Marzari, *Phys. Rev. B* **71**, 205214 (2005).
25. J. Röhl, M. Hundhausen, K. V. Emtsev, Th. Seyller, R. Graupner, and L. Ley, *Appl. Phys. Lett.* **92**, 201918 (2009).
26. J. J. Neumeier, T. Tomita, M. Debessai, J. S. Schilling, P. W. Barnes, D. G. Hinks, and J. D. Jorgensen, *Phys. Rev. B* **72**, 220505 (2005).
27. J. L. MacManus-Driscoll, *Nature Materials* **7**, 315 (2008).

Table I: The full width at half maximum (FWHM) of the (110) peak, the lattice parameters, and the transition temperature (T_c) for the MgB₂ samples, made with 0, 3.7, and 8.7 at% graphene doping via a diffusion process.

Sample	Lattice Constants			Grain Size (nm)	Strain (%)	FWHM (110) (°)	T _c (onset) (K)
	a (Å)	c (Å)	c/a				
G000	3.084(1)	3.525(1)	1.143(1)	216(10)	0.1198(188)	0.288	38.9
G037	3.082(1)	3.527(1)	1.144(1)	170(8)	0.1685(250)	0.400	37.7
G087	3.075(1)	3.525(1)	1.146(1)	171(11)	0.1782(330)	0.414	36.7

Figure Captions:

Figure 1: The temperature dependence of the resistivity (ρ) measured in different fields for doped and undoped samples.

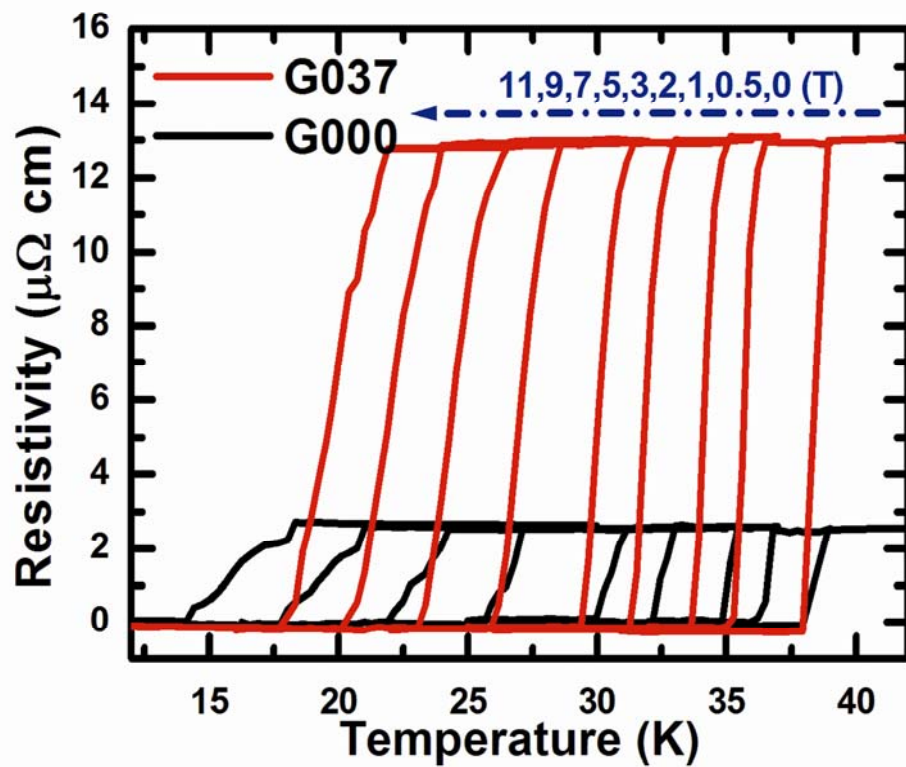


Figure 2: Critical current density as a function of magnetic field at 5 K and 20K for with and without graphene doped samples. 5 at% nano-C doped sample for a comparable result at the same sample preparation route.

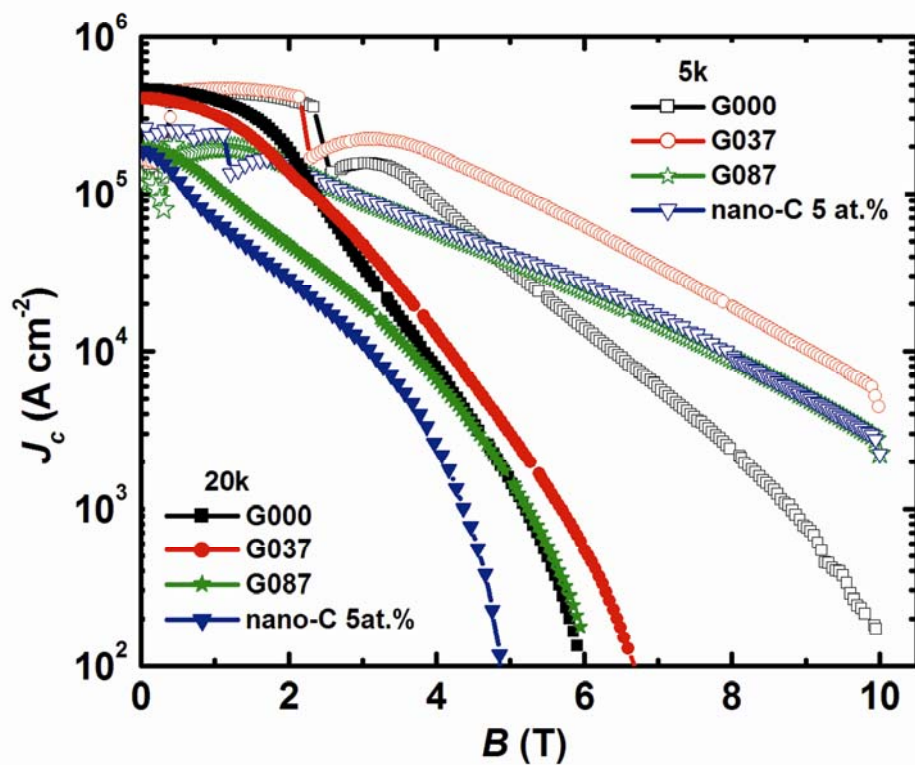


Figure 3: Upper critical field, H_{c2} , and irreversibility field, H_{irr} , versus normalised transition temperature, T_c , for all graphene doped and undoped MgB₂ samples.

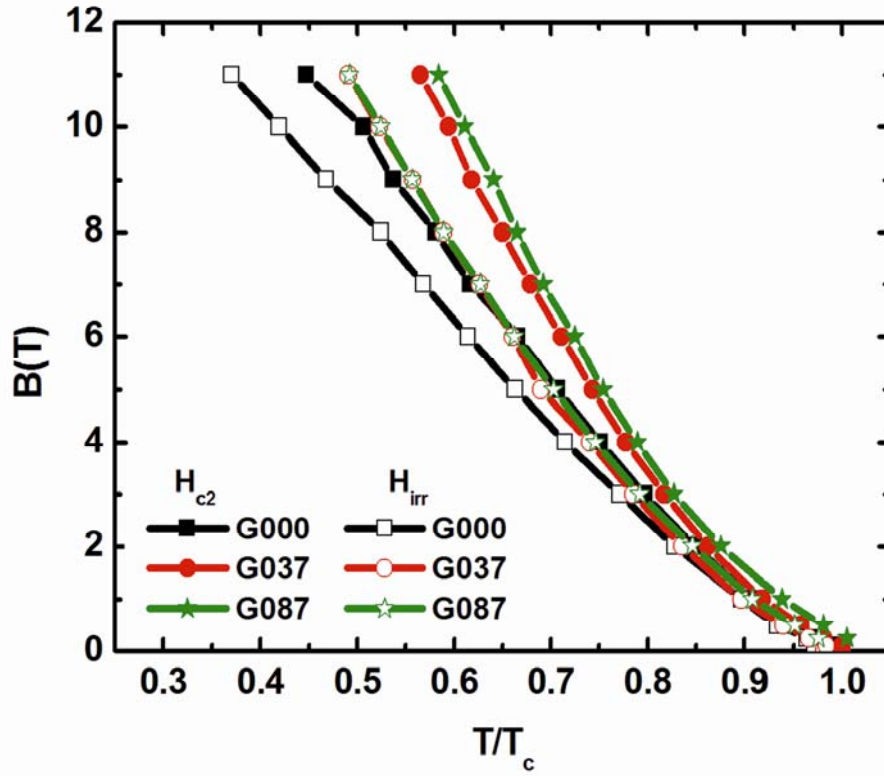


Figure 4: (a) TEM image showing the defects with grains of the G037 sample with order of fringes varies between grains. Defects and fringes are indicated by arrow, and (b) HRTEM image of fringes. TEM images show large amount of defects and fringes can be observed in the graphene doped sample G037. (c) TEM image of the undoped sample for reference.

